Supporting Information

Bifunctional and Regenerable Molecular Electrode for Water Electrolysis at Neutral pH

Biswanath Das,* [a] Esteban Alejandro Toledo-Carrillo,[b] Guoqi Li,[c] Jonas Ståhle,[a] Thomas Thersleff,[d] Jianhong Chen,[d] Lin Li, Fei Ye,[b] Adam Slabon,[e] Mats Göthelid ,[f] Tsu-Chien Weng,[c] Jodie A. Yuwono, [g] Priyank V. Kumar,[g] Oscar Verho,* [h] Markus D. Kärkäs,[i] Joydeep Dutta ,[b] and Björn Åkermark* [a]

Dr. Biswanath Das, Dr. Jonas Ståhle, Prof. Björn Åkermark
Department of Organic Chemistry, Arrhenius Laboratory
Stockholm University, Svante Arrhenius väg 16C, 10691 Stockholm, Sweden.
E-mail: das.biswanath85@gmail.com/biswanath.das@su.se, bjorn.akermark@su.se

[b] Mr. Esteban A. Toledo-Carrillo, Dr. Fei Ye, Prof. Joydeep Dutta
Department of Applied Physics, KTH Royal Institute of Technology,
Hannes Alfvéns väg 12, 114 19 Stockholm, Sweden

[c] Mr. Guoqi Li, Dr. Lin Li, Prof. Tsu-Chien Weng
School of Physical Science and Technology, ShanghaiTech University,
Shanghai 201210, China

[d] Dr. Thomas Thersleff, Mr. Jianhong Chen
Department of Materials and Environmental Chemistry,
Stockholm University, Svante Arrhenius väg 16C, 10691 Stockholm, Sweden

[e] Professor Dr. Adam Slabon
Inorganic Chemistry, University of Wuppertal
Gaußstr. 20, 42119 Wuppertal, Germany

[f] Prof. Mats Göthelid
Material and Nanophysics, KTH Royal Institute of Technology,
Hannes Alfvéns väg 12, 114 19 Stockholm, Sweden

[g] Dr. Jodie Yuwono, Asst. Prof. Priyank V Kumar
School of Chemical Engineering, University of New South Wales,
Sydney 2052, Australia

[h] Assoc. Prof. Oscar Verho
Department of Medicinal Chemistry, Biomedicinskt Centrum BMC,
Uppsala University, SE-75123 Uppsala, Sweden
E-mail: oscar.verho@ilk.uu.se

[i] Assoc. Prof. Markus D. Kärkäs
Department of Chemistry, KTH Royal Institute of Technology,
SE-10044 Stockholm, Sweden

Methods and Materials:

All reagents and solvents were commercially available and used as received, unless otherwise noted. Reagent grade organic solvents were used for the purification and HPLC grade solvents were used for synthesis and other operations.

NMR spectra were recorded on a Bruker Avance II 500 MHz spectrometer using a 5 mm BBO probe equipped with Z-gradients. Peaks were referenced to the internal solvent peaks (δH 3.31 for MeOD).

HRMS spectra were recorded in positive mode on a Bruker Daltonics MicrOTOF mass spectrometer using electrospray ionization as the ion source. The peaks were referenced to a serially injected sample of 10 mM sodium formate. The data was exported and presented using GNU Octave. ESI-HRMS measurements were performed using the Bruker Daltonics microTOF mass spectrometer (direct injection, positive mode, all samples in MeOH).

Unless otherwise mentioned, all the DFT calculations were implemented using the Vienna ab-initio simulation package (VASP) [1,2] with the core and valence electronic interactions being modelled using the projector augmented wave (PAW) method[3,4]. The Perdew-Burke-Ernzerhof (PBE) exchange-correlation functional[5] was employed. The wavefunction were expanded with a kinetic energy cut-off of 500 eV and a Gamma k-points were used. Geometrical optimizations were achieved by relaxing all ionic position and supercell vectors until the Hellman-Feynmann forces were less than 0.01 eV $Å^{-1}$. The dispersion correction was also considered in this study by using DFT-D3 method[6]. The Gibbs reaction energy were computed using the contribution of adsorption reaction energy and zero-point energy at 298 K and solvation corrections for each system[7].

Additional Characterization details:

Electron microscopy study:

A collection of aggregates was located on the TEM grid and an overview of this is presented in Figure S10a. This region was scanned with a focused electron probe to simultaneously collect hyperspectral data cubes containing Energy Dispersive X-Ray (EDX) as well as low-loss and core-loss Electron Energy-Loss Spectra (EELS). The EDX spectrum extracted by integrating over the entire aggregate is presented in Figure S10f. While this spectrum is displayed in the energy range from 0 – 3 keV, data were collected up to 20 keV, permitting use of the Ru-K_{α} edge, which was used for quantification. Carbon, Nitrogen, Oxygen, and Ruthenium are all clearly retrieved. Additional peaks corresponding to Aluminium, Zinc, and Sulfur are likely impurities introduced in low concentrations during the sample preparation routine, while the Copper signal originates from the TEM grid. The catalyst composition estimated from this EDX spectrum is presented in Table S1 below and reveals that Ru is found in concentrations of less than 1 AF%. It should be noted, since this EDX spectrum is integrated over the entire field of view, it will contain additional Carbon and Oxygen contributions from hydrocarbon contamination and the support film.

Small quantities of Al, Cu and Zn were also found in the EDX spectra (Figure S10b). These elements come from the metal salts used during the activation of the carbon fibers by wet impregnation and carbonization.[8,9]

The background subtracted spectrum is presented in blue and this was subsequently deconvolved using the simultaneously acquired electron energy loss spectroscopy (EELS) to remove plural scattering, as shown in the red spectrum in the foreground. In Figure S10f-g, an EELS spectrum extracted from a thin region of the aggregate is presented. The raw EELS data are shown in green along with the pre-edge background, which was modelled with an inverse power law function in the energy range 250 – 275 eV. A very prominent C-K edge including some interesting fine structure features dominates this spectrum. In addition, weak intensities at the onset energies for N-K, O-K, and Ru-$M_{4,5}$ were observed.

Additional peaks in the EDX analysis corresponding to Aluminium, Zinc, and Sulfur are likely impurities introduced in low concentrations during the sample preparation routine, while the Copper signal originates from the TEM grid.

The catalyst composition estimated from this EDX spectrum is presented in Table S1 below and reveals that Ru is found in concentrations of less than 1 AF%. It should be noted, since this EDX spectrum is integrated over the entire field of view, it will contain additional Carbon and Oxygen contributions from hydrocarbon contamination and the support film.

Small quantities of Al, Cu and Zn were also found in the EDX spectra (Figure S10b). These elements come from the metal salts used during the activation of the carbon fibers by wet impregnation and carbonization.[8,9]

The background subtracted spectrum is presented in blue and this was subsequently deconvolved using the simultaneously acquired electron energy loss spectroscopy (EELS) to remove plural scattering, as shown in the red spectrum in the foreground.

X-ray photoelectron spectroscopy

In addition to the discussion in the manuscript, higher carbon loading of catalysts intensifies the carbon peaks and reduces the peak corresponding to CF_2 units. Additionally, the shoulder that can be observed around 293 eV indicates a perturbation in the C-F surrounding due to the anchoring of the catalyst structure.

UV-Vis spectroscopy- The identity of the molecular catalyst onto the carbon cloth was tested by UV-Vis before and after the electrolysis by immersion in either a highly acidic (1.0M HCl) or alkaline solution (1.0M KOH) for 24 h (Figure S22). The acid and alkaline solution were analyzed using UV-Vis spectrometer Lambda750 (PerkinElmer) to detect the presence of molecular catalyst after dissolution. Similarly, the concentration of Ru was measured by Inductive Coupled Plasma Optical Emission Spectroscopy (ICP-OES) using iCAP 6500 spectrometer (Thermo Scientific).

Fourier Transform Infrared Spectroscopy (FTIR) using a Nicolet iS10 Spectrometer (Thermo Scientific) equipped with an ATR accessory. Figure S10 shows the FTIR spectra of treated and untreated carbon cloth, and in these, a characteristic band assigned to aromatic C=C stretching can be observed at 1520 cm^{-1}.[10] A strong and broad band appeared after fluorination of carbon cloth at about 1070 cm^{-1}, which corresponds to the stretching of C-F bonds, and this band was present in all the treated samples.[11] No additional signal could be observed after pyridine ligand grafting, which was most likely due to the small amount incorporated. However, anchoring of the pyridine linker was confirmed by XPS *(vide supra).* The absence of new features in the spectra confirmed that no significant degradation took place during the surface modification. After anchoring of the molecular catalyst, a weak band was found at 1718 cm^{-1}, corresponding to C=O stretching of the carboxylate unit in the Ru complex. Furthermore, a weakening of the C-F stretching band was observed after catalyst anchoring, which was in line with the changes of the C-F peak in the XPS spectra. These observations, together with the presence of new C-F bands at about 293 eV in the XPS spectra, suggest chemical interaction between fluorine and the atoms of the molecular catalyst. These interactions can most likely be ascribed to hydrogen bonding between the fluorines of the PFCC and the protons of the water molecule in the molecular catalyst.

Raman spectral analysis

All samples displayed two prominent bands at 1330 and 1600 cm^{-1} and a broad band centered at about 2500 cm^{-1}, which were attributed to first and second order Raman scattering of carbonaceous materials (Figure S11). The Raman active mode of highly ordered carbon material corresponds to the G band centered at 1580 cm^{-1}, assigned to the in-plane E_{2g} vibrational mode. However, in activated carbon fibers, a highly disordered structure is present, giving rise to a new strong set of bands in the spectra, which is usually denoted as the D bands. A more detailed analysis shows that the D and G bands can be deconvoluted into four different signals, which arise from different type of disordered regions in the carbon fibers. The blue shift observed in the G band is most likely related to the unresolved overlapping with the D_2 band (1610 cm^{-1}). The D_1 band corresponds to an in-plane transverse optical (TO) mode (Raman inactive mode), which appears when defects are present in the graphitic plane and is usually considered as a measure of the graphitization degree through the intensity ratio I_D/I_G or the area ratio A_D/A_G. Two other modes at about 1180 and 1530 cm^{-1}, the so-called D_4 and D_3 bands, are normally associated with amorphous regions and out-of-plane vibrations due to heteroatoms grafted on graphite units.[12] The analysis revealed the effect of fluorine doping on the degree of graphitization. A significant increase in the area ratio A_D/A_G from 3.11 to 3.54 has been reported earlier to be due to the creation of defective sites in the sp^2 carbon plane following HF treatment.[13] Additionally, an increase in the intensity of the D_3 band (A_{D3}/A_G increase from 1.81 to 2.66) is associated with the incorporation of out-of-plane CF_2 groups.[14] In contrast, no significant disorder was observed upon grafting of the pyridine ligand onto FCC (A_D/A_G decrease from 3.54 to 3.53), since out-of-plane surface functionalities do not increase the intensity of the D bands.[15] Unlike fluorination, the pyridine modification procedure was carried out in a reductive environment. Thus, the defect density in the crystalline regions of the carbon fibers most likely remained unchanged. After the Ru catalyst anchoring process, a new but weak band at about 450 cm^{-1} appeared that was assigned to Ru-O and Ru-N bonds present in the molecular catalyst, which presents further evidence of the successful immobilization of the Ru catalyst.

Thermogravimetric study

The results of the thermogravimetric analysis are shown in Figure 2e and S14. Fluorine-doped carbon cloth shows similar behavior as the untreated carbon cloth in the temperature range of 150-500°C with a partial weight loss (of ~ 2%), which can be attributed to the removal of physi-adsorbed water, and carboxyl and hydroxyl groups.[16-17] For temperatures above 500°C, a single peak is present for CC and FCC in the differential thermal analysis (DTA) (Figure S13), centered at 559 and 591°C respectively, indicating a complete degradation of the carbon structure due to thermal oxidation. The increase in degradation temperature of the FCC can be attributed to the introduction of C-F bonds onto the surface of the fibres, which makes the available carbon sites more resilient to oxidation.[18]

Upon grafting of the -CH_2-CH_2-pyridine units onto the surface of the carbon fibers, a two-stage degradation is observed with a partial weight loss of 5.74% in the temperature range of 200-400°C, which is attributed to thermal desorption of the ligand (pyridine-carbon chain).[19] No noticeable change in the complete degradation temperature is observed with respect to FCC, indicating that the new surface functional groups grafted do not weaken the C-F bonds that are responsible for the oxidative resistance of the electrode.

Thermogravimetric analysis shows a clear difference between PFCC and RuPFCC (Figure 2e). Immobilization of the Ru catalyst, causes an increase in weight loss in the temperature range from 200-400°C. As shown in the inset in Figure 2e, the weight loss corresponds to 8.95% for RuPFCC. The difference in the weight loss observed in the thermogravimetric analysis, compared to the loading mass obtained after each preparation procedure is most likely related to the hydrogen-bonded water molecules attached to the catalyst.

Electrochemical Characterization and reactivity study

The electrochemical setup consists of a platinum wire as the counter electrode, Ag/AgCl (3.0 M KCl) as the reference electrode, and the carbon cloth samples as the working electrode. The solution employed was 0.1 M of phosphate buffer solution (pH 7). Prior to each measurement, the samples were immersed until stable potential was reached. Cyclic voltammetry behavior of the electrodes was tested in a wide potential scale (+2.25 V to -1.0 V vs RHE) and the operating potential for the bulk electrolysis (controlled potential electrolysis) experiments for water oxidation were selected. Electrochemical Impedance Spectroscopy (EIS) was performed in potentiostatic mode at open circuit potential (bias potential) within a frequency range from 100 kHz to 10 mHz with a perturbation of 10 mV rms.

Chronopotentiometric experiments and gas detection

CPE experiments were conducted to confirm the oxidation of water, and reduction of protons. These experiments also allow evaluating the stability of the anchored catalyst. For oxygen evolution a constant current of 2.6 mA/cm^2 and for hydrogen production, a constant current of -5 mA/cm^2 was applied over 120 min to a RuPFCC working electrode (1cm x 1cm). The experiments were performed in a 0.1M Phosphate Buffer Solution pH 7, with a carbon counter electrode and Ag/AgCl as reference electrode The dissolved gas was detected in a closed system using an O_2 and H_2 measurement system (Unisense) comprising a needle sensor of 2.1 x 80mm connected to an O_2 and H_2 UniAmp units. Prior to starting the experiment, the system was purged with N_2 for 30 min.

Electrode regeneration of the electrode (ERE). After oxidation processes (long CPE experiments), the electrochemical behavior of the electrodes was checked under nitrogen. In almost all the cases slight increase in the overpotential and decrease in the WO current were observed. Envisioning that the oxidative stress of the continuous positive potential onto the electrode can be a reason, electrodes were reduced for 2h/4h duration (depending on the time of oxidation) under CPE condition. The potentials for CPE experiments were chosen from the electrochemical behavior of the electrodes after oxidation experiments. The chosen value of the fixed potential for the regeneration (reduction) experiments were the potentials where it started proton reduction behavior. Upon reduction, regeneration of electrocatalytic WO activity was found to be up to ~98% after 48 h use and of ~70% after 16 days.

Calculation of turnovers (TO).

For **water oxidation**, TO_{WO} = number of moles of water oxidized/(mole of catalyst)

TO_{WO} is calculated from the charge vs time plot of the CPE experiments.

At the WO potentials, e.g., at +1.71 V (for 8 h) and 1.81 V (for 48 h) (vs RHE) charge transfer of 7.2 coulombs and 30.6 coulombs were seen respectively. (1 mA.h = 3.6 coulomb)

96500 coulomb = 1 mole of electrons

7.2 coulomb = 7.46×10^{-5} mole of electrons ≡ oxidation of 3.73×10^{-5} mole of water (transfer of 4 electrons is needed to oxidize 2 water molecules)

30.6 coulomb = 3.17×10^{-4} mole of electrons ≡ oxidation of 1.59×10^{-4} mole of water

To minimize the error of calculating the catalyst amount on PFCC, the same procedure was repeated ten times and an average was taken into consideration. A total amount of 2.1 mg of catalysts lost from the stock solution was observed after anchoring **1** onto ten batches of 3 cm x 3 cm PFCC electrode. Each PFCC contains approximately 0.21 mg of **1**.

i.e. a 1 cm x 0.5 cm electrode (used for CPE) contains (0.21 x 0.5) / 9 mg = 0.0116 mg = 2.14×10^{-8} mole (MW of $1+H_2O$ is 545.03) of **1**

TO_{WO} over 8 h at 1.71 V (vs RHE) is $(3.73 \times 10^{-5}) / (2.14 \times 10^{-8}) = 1742.9$ and >95% recovery of the electrocatalytic activity was possible after regeneration process.

TO_{WO} over 48 h at 1.81 V (vs RHE) is $(1.59 \times 10^{-4}) / (2.14 \times 10^{-8}) = 7429.9$ and >90% recovery of the electrocatalytic activity was possible after regeneration process.

For **proton reduction**, TO_{PR} = number of moles of water reduced/(mole of catalyst)

TO_{PR} is calculated from the charge vs time plot of the CPE experiments.

At the PR potentials, e.g., at -0.79 V (for 3 h) (vs RHE) charge transfer of 7.6 coulomb was observed. (1 mA.h = 3.6 coulomb)

96500 coulomb = 1 mole of electrons

7.2 coulomb = 7.88×10^{-5} mole of electrons ≡ reduction of 7.88×10^{-5} mole of protons

1 cm x 0.5 cm electrode (used for CPE) contains 2.14×10^{-8} mole (see above; MW of $1+H_2O$ is 545.03) of **1**.

TO_{PR} over 3 h at -0.79 V (vs RHE) is $(7.88 \times 10^{-5}) / (2.14 \times 10^{-8}) = 3682.2$

Calculation of the weight percentage of ruthenium on RuPFCC. According to our investigations (see above), 0.21 mg of 1 [$Ru^{II}(mcbp)(H_2O)_2$] was used for the preparation of a RuPFCC electrode with a 3 cm x 3 cm diameter. Since the catalyst was anchored as [$Ru^{II}(mcbp)(H_2O)$] (after replacing one H_2O unit), 0.203 mg [$Ru^{II}(mcbp)(H_2O)_2$] should be considered for the quantitative analysis. In [$Ru^{II}(mcbp)(H_2O)$] the weight percentage of ruthenium is (101.9/545.03) x 100% = 18.69%, i.e., in 0.203 mg of [$Ru^{II}(mcbp)(H_2O)$] the quantity of ruthenium is 0.038 mg. The total weight of the 3 cm x 3 cm diameter of RuPFCC electrode was 101.4 mg. Thus, the weight percentage of ruthenium on the RuPFCC electrode is (0.038/101.4) x 100% = 0.037%

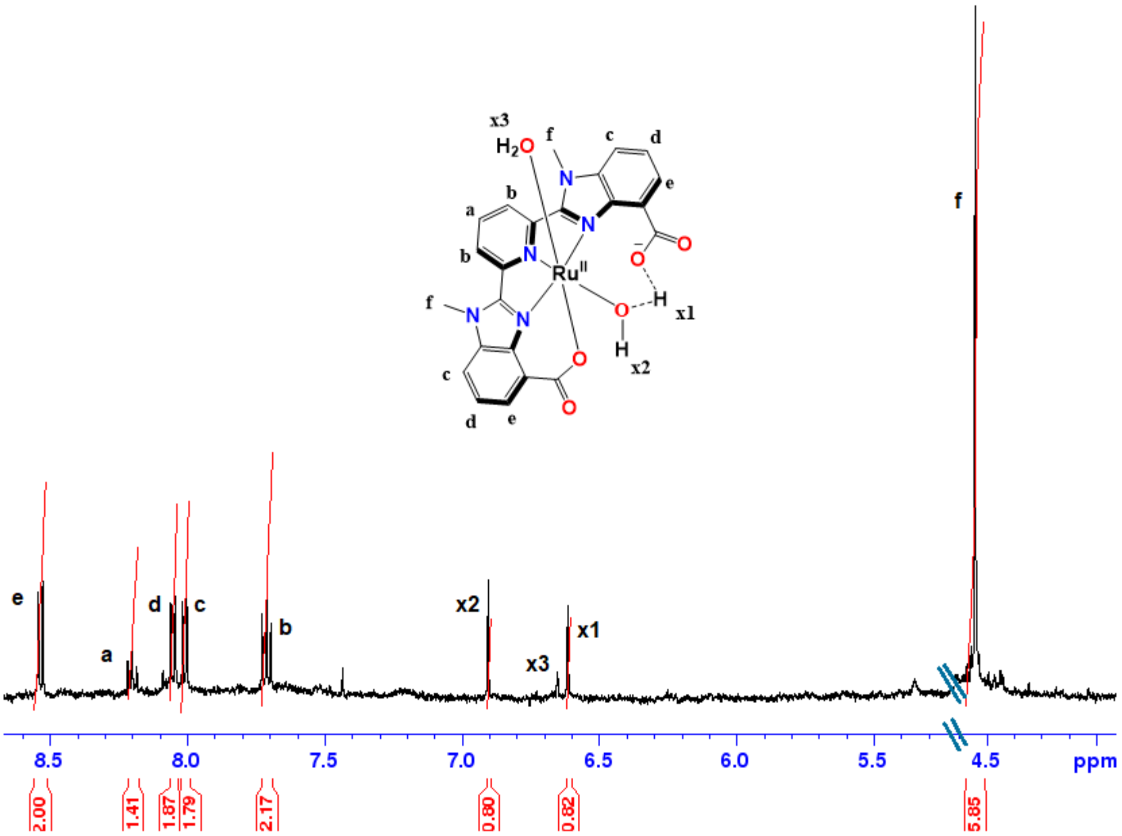

Figure S1. 500 MHz, ^{1}H NMR (4.0-8.6 ppm) of **1** in CD_3OD at 298 K. Inset shows chemical structure of **1**. Broad singlet signal of non-coordinated water at 4.87 ppm is deleted for clarity.

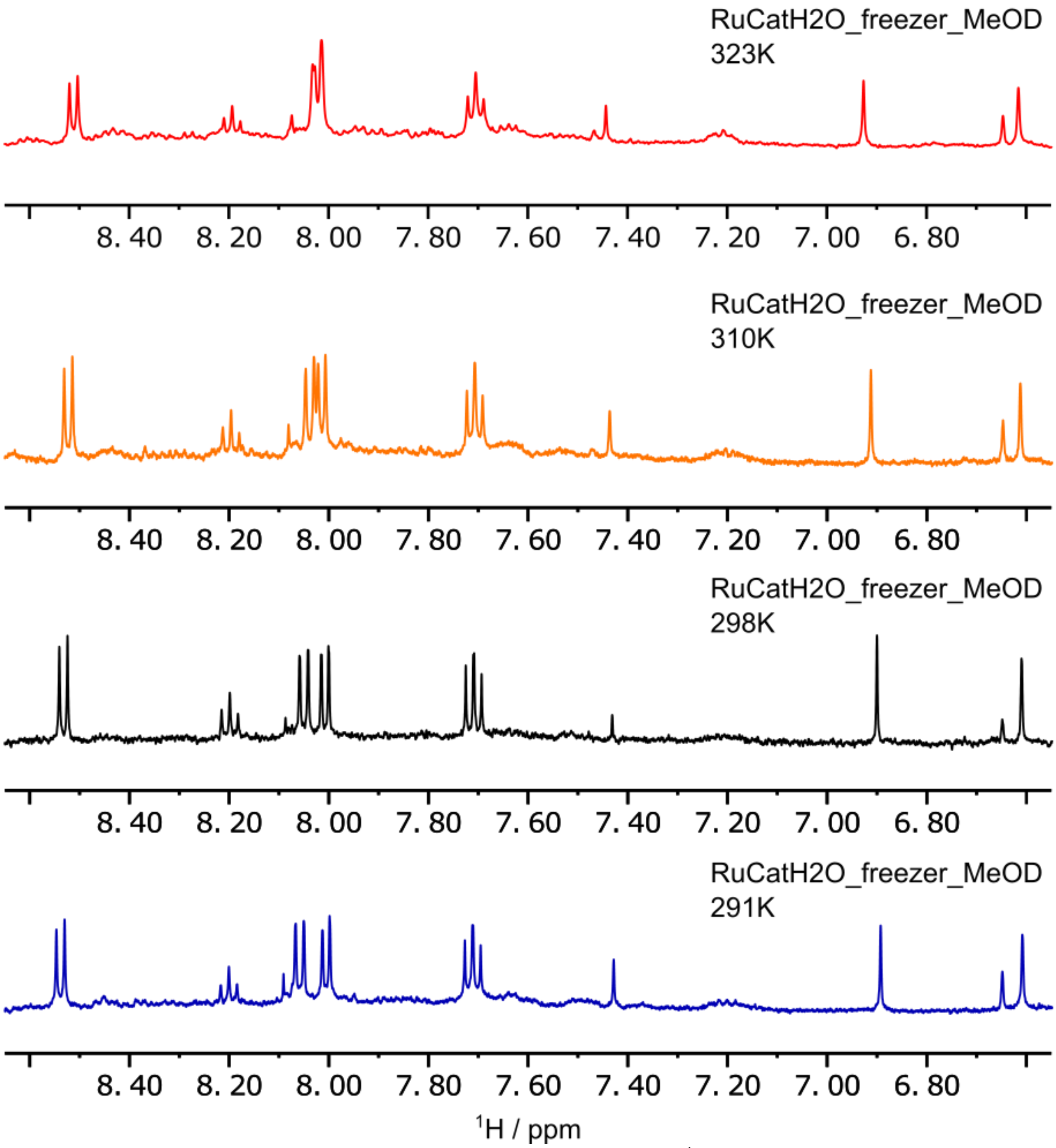

Figure S2. 500 MHz, temperature dependent (291 K-232 K) ^{1}H NMR (6.6-8.6 ppm) of **1** in CD_3OD.

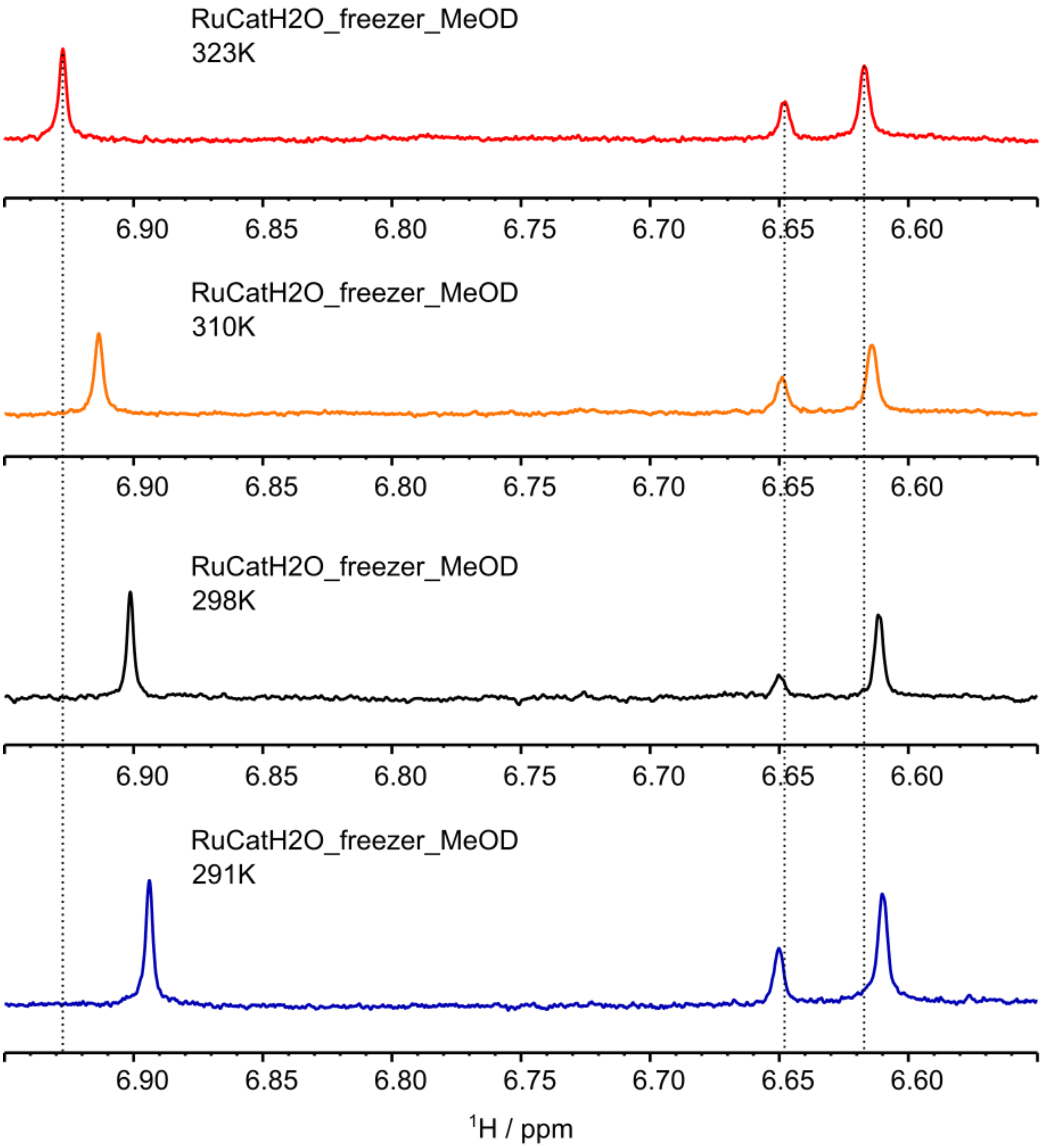

Figure S3. Magnified 500 MHz, temperature dependent (291 K-323 K) ^{1}H NMR (6.55-6.95 ppm) of **1** in CD_3OD, showing clear difference in temperature dependence depending on whether the proton is H-bonded or free.

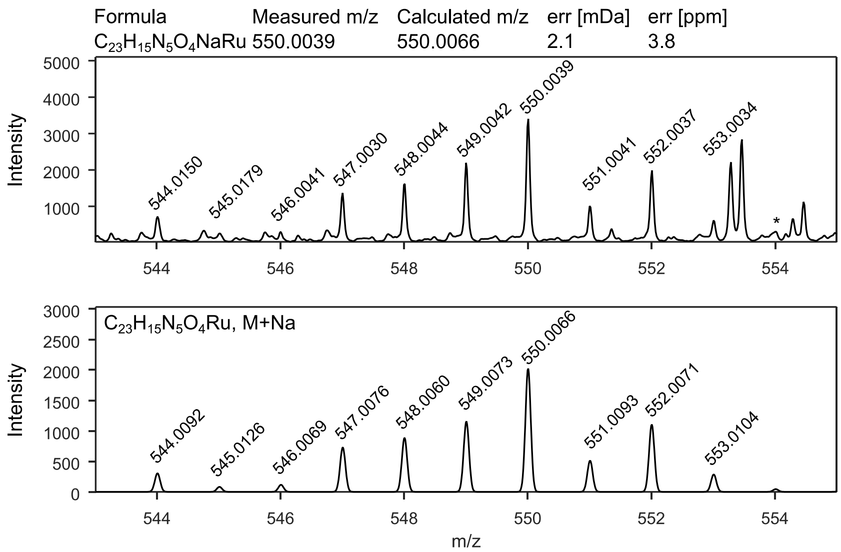

Figure S4. Experimental isotope pattern of the major singly charged species at 550.0039 from an HRMS experiment of a methanol solution of **1** and corresponding calculated isotope pattern of the molecular formula $C_{23}H_{15}N_5O_4RuNa$ (**1**+Na^+) at 550.0066. An asterisk signifies a peak obscured by overlapping signals.

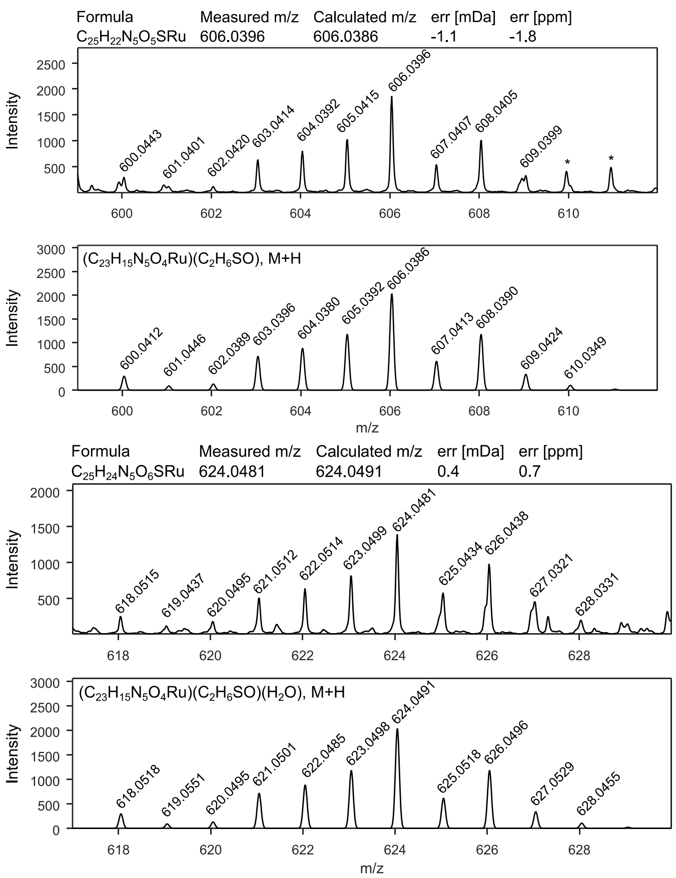

Figure S5. Experimental isotope pattern of two singly charged species at 606.0396 and 624.0481 from an HRMS experiment of a methanol:H_2O:DMSO solution of **1** and corresponding calculated isotope patterns of the molecular formulas $C_{25}H_{21}N_5O_5SRuH$ (**1**+DMSO+H^+) at 606.0386 and $C_{25}H_{23}N_5O_6SRuH$ (**1**+DMSO+H_2O+H^+) at 624.0491. The easily detectable DMSO and water coordination points towards the vacant site available on the ruthenium center in **1**, that is essential for catalyst anchoring and catalysis. An asterisk signifies a peak obscured by overlapping signals.

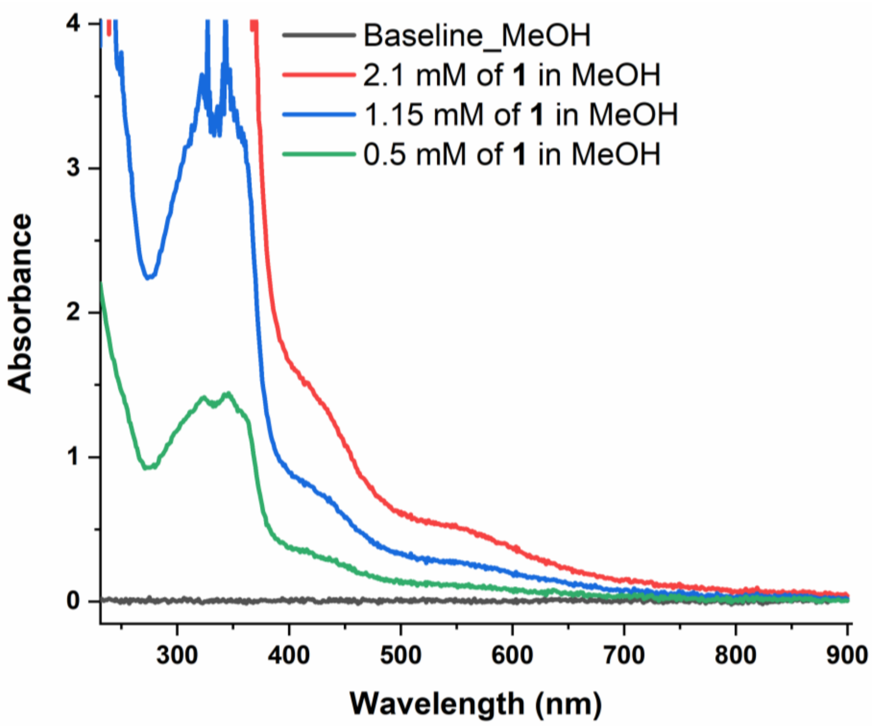

Figure S6. UV-Vis spectra (240–900 nm) of a methanol solution of **1** in different concentrations (0.5 mM – 2.1 mM).

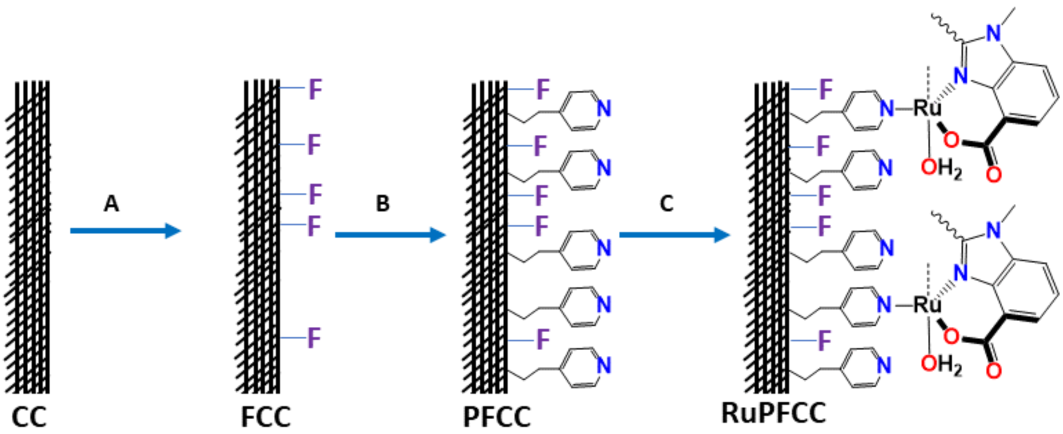

Figure S7. Schematic representation of the stepwise preparation of RuPFCC. Detail procedure is discussed in the experimental section. A is 20% HF, B is a combination of 4-(2-aminoethyl) pyridine, HBF_4, CH_3COOH and isoamyl nitrite, C is **1** in MeOH:H_2O (1:1).

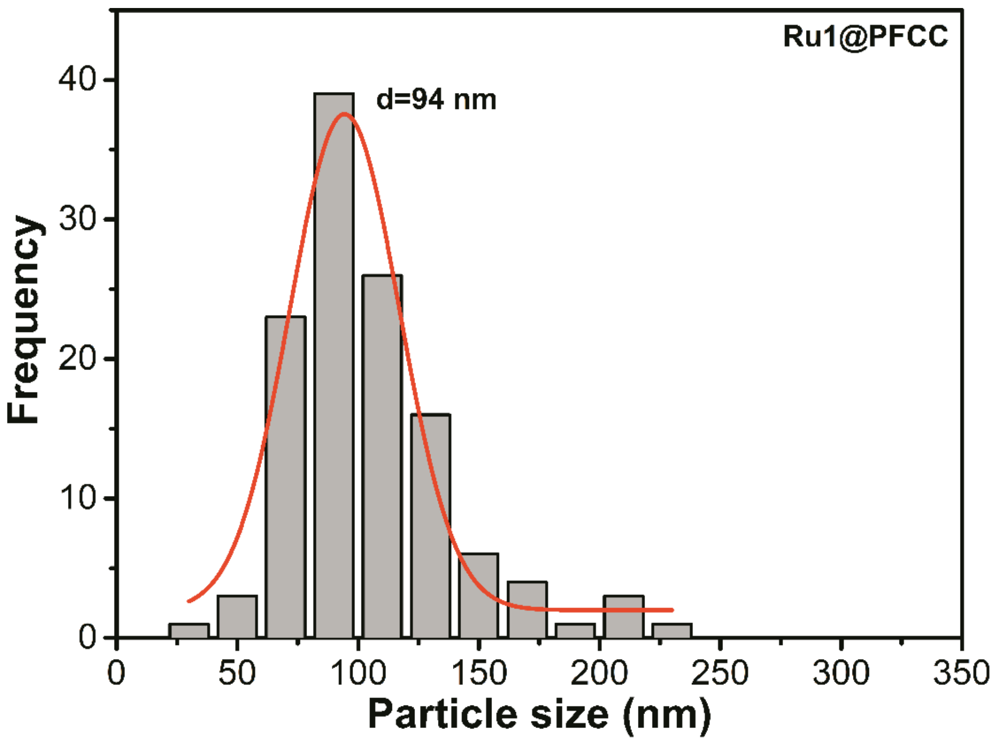

Figure S8. Agglomeration size histogram calculated from SEM images

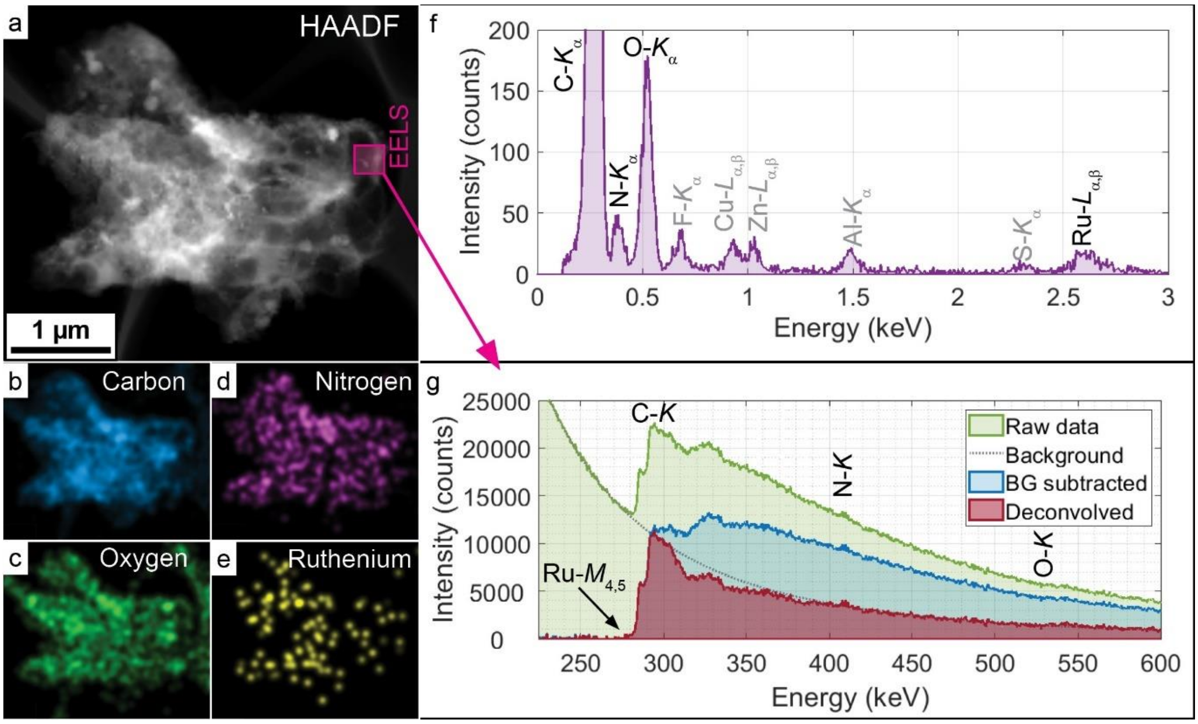

Figure S9. Results of the TEM investigation. In (a), a Z-contrast scan of a collection of aggregate is presented. EDX maps from this region are presented in false color for Carbon (b), Oxygen (c), Nitrogen (d), and Ruthenium (e). In (f), the integrated EDX spectrum from the entire field of view is presented along with peak labels. Grey peaks were identified as impurities. In (g), an EELS spectrum from the boxed region in (a) is presented. Pre-edge background and plural scattering contributions are removed in the red spectrum presented in the foreground.

Table S1 – EDX quantification results from the spectrum presented in **Figure S12f**

Element	**Quantification edge family**	**Atomic Fraction (%)**	**Mass Fraction (%)**
C	*K*	88.63 ± 3.20	82.44 ± 1.85
N	*K*	2.73 ± 0.56	2.96 ± 0.60
O	*K*	8.05 ± 1.64	9.98 ± 2.01
Ru	*K*	0.59 ± 0.10	4.62 ± 0.78

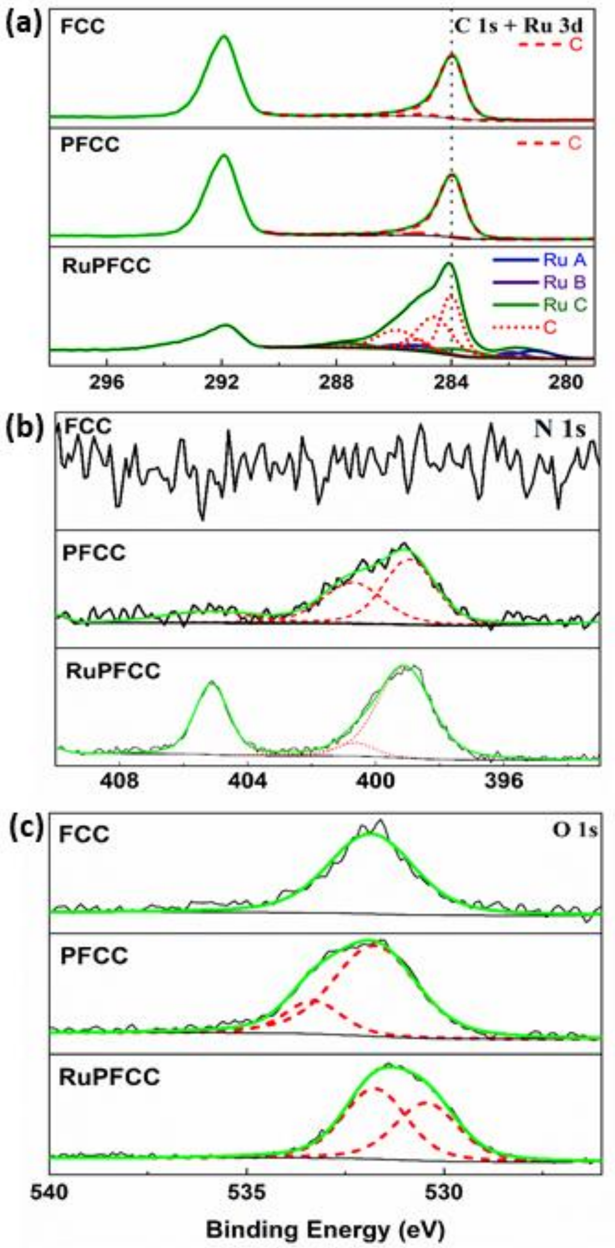

Figure S10. High-resolution XPS spectra of (a) C 1s + Ru 3d , (b) N 1s and (c) O 1s. Sample 1, Sample 2 and sample 3 represents FCC, PFCC and RuPFCC respectively.

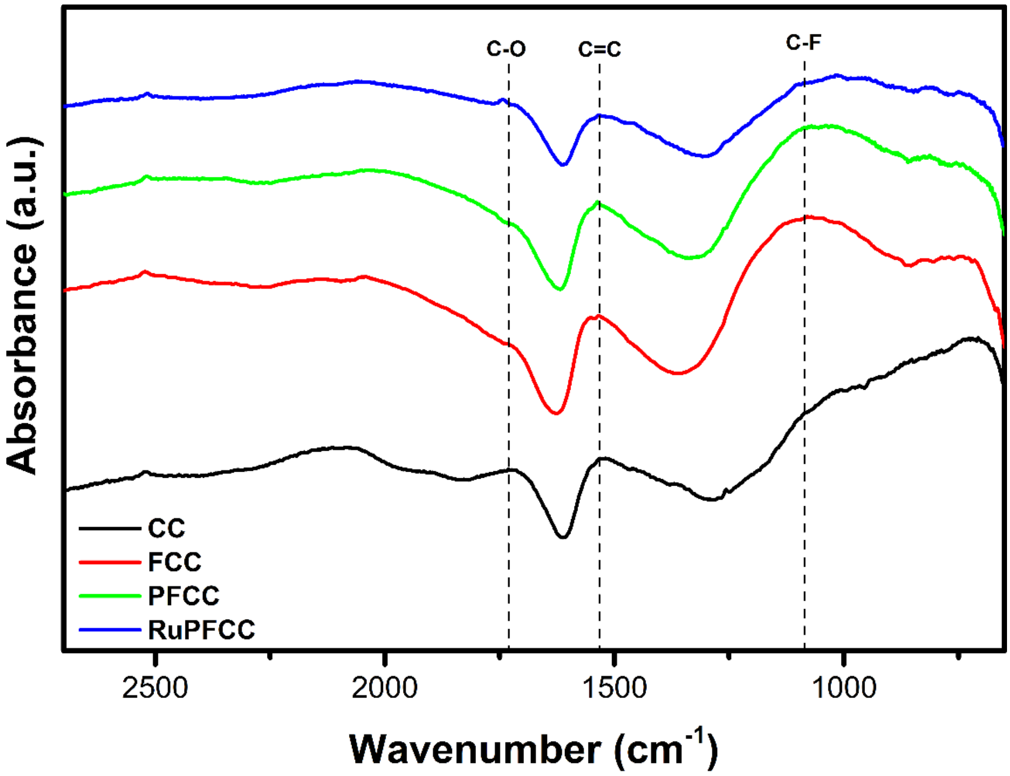

Figure S11. FTIR spectra of pristine activated carbon cloth (CC), fluorinated (FCC), pyridine modified (PFCC) and Ru catalyst anchored (RuPFCC) carbon cloth.

Table S2. Deconvolution parameter of Raman spectra for CC, FCC, PFCC and RuPFCC samples.

Sample	**D_4**		**D_1**		**D_3**		**$G+D_2$**		**A_D/A_G**
	Position	FWHM	Position	FWHM	Position	FWHM	Position	FWHM	
CC	1185.1 ± 6.3	85.3 ± 15.3	1324.5 ± 1.1	67.4 ± 1.3	1518.8 ± 5.8	97.6 ± 8.7	1599.2 ± 0.3	28.4 ± 1.2	3.15
FCC	1186.6 ± 12.8	99.7 ± 15.1	1327.8 ± 2.5	68.9 ± 4.3	1526.8 ± 8.7	111.5 ± 22.5	1597.1 ± 2.0	28.3 ± 1.1	3.54
PFCC	1180.2 ± 9.2	94.1 ± 11.6	1327.8 ± 1.5	71.2 ± 2.6	1528.8 ± 10.2	96.9 ± 11.9	1599.3 ± 1.1	27.8 ± 0.9	3.53
RuPFCC	1178.2 ± 3.1	90.4 ± 15.5	1329.9 ± 1.5	73.6 ± 1.7	1531.3 ± 5.9	95.7 ± 7.2	1601.7 ± 0.6	28.1 ± 1.2	3.79

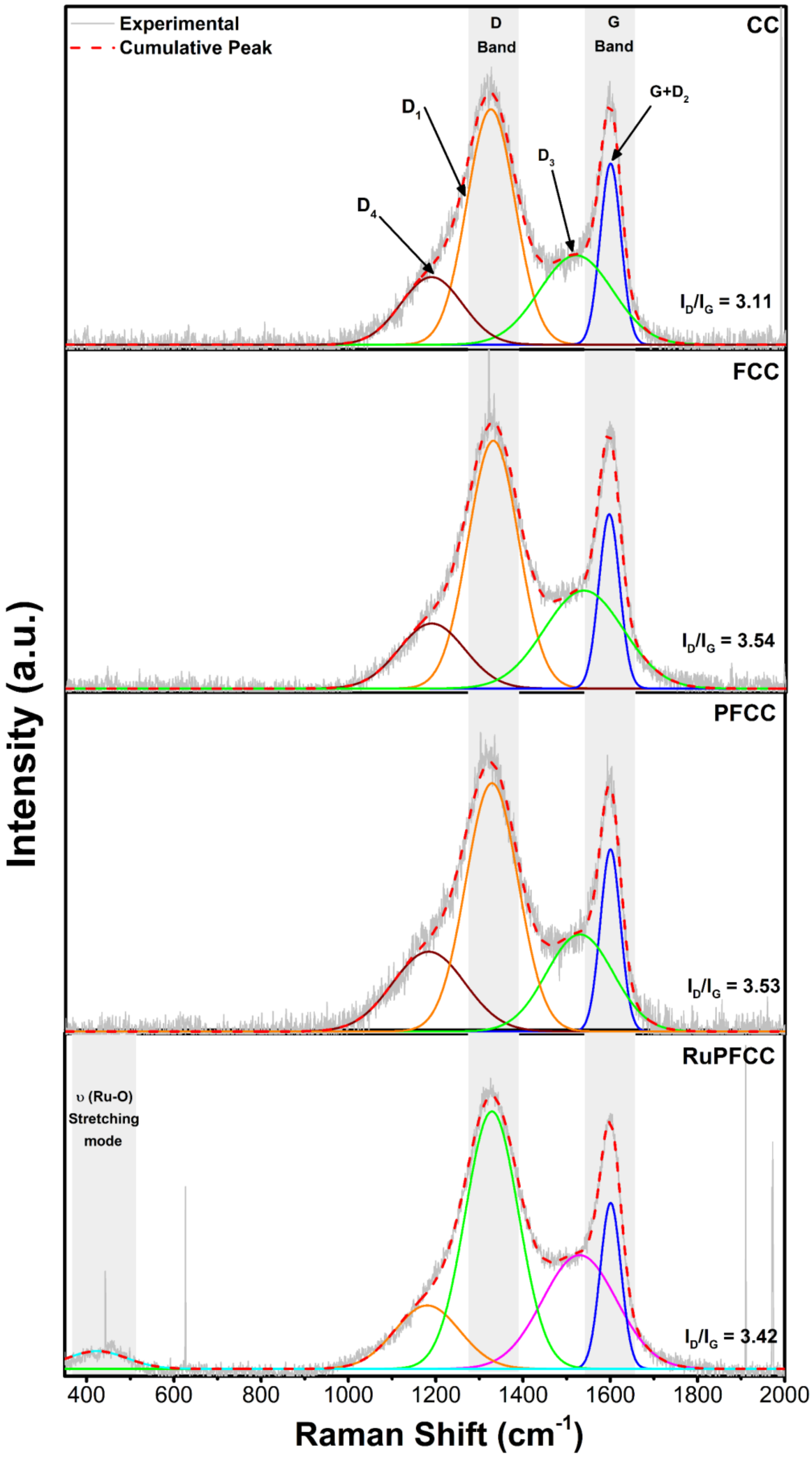

Figure S12. Deconvolution of Raman spectra of pristine activated carbon cloth (CC), fluorinated (FCC), pyridine modified (PFCC) and Ru catalyst anchored (Ru PFCC)

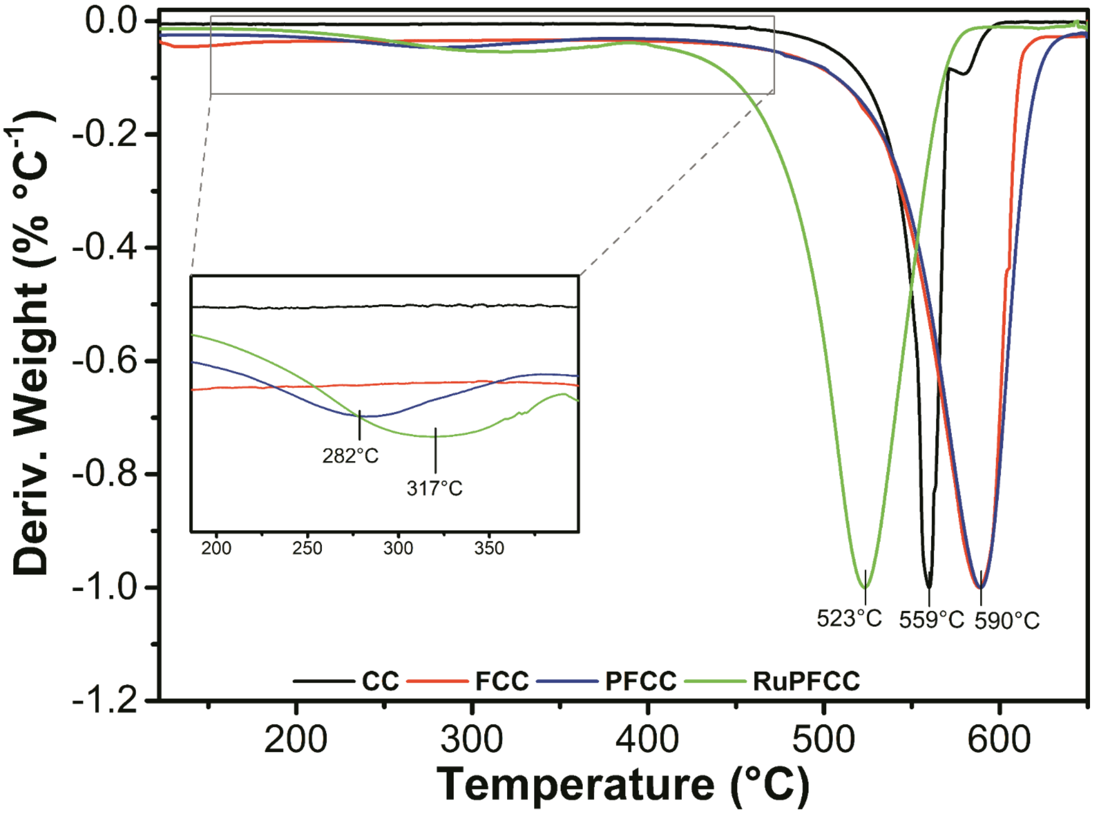

Figure S13. Differential Thermal Analysis under air flow for untreated and treated carbon cloth.

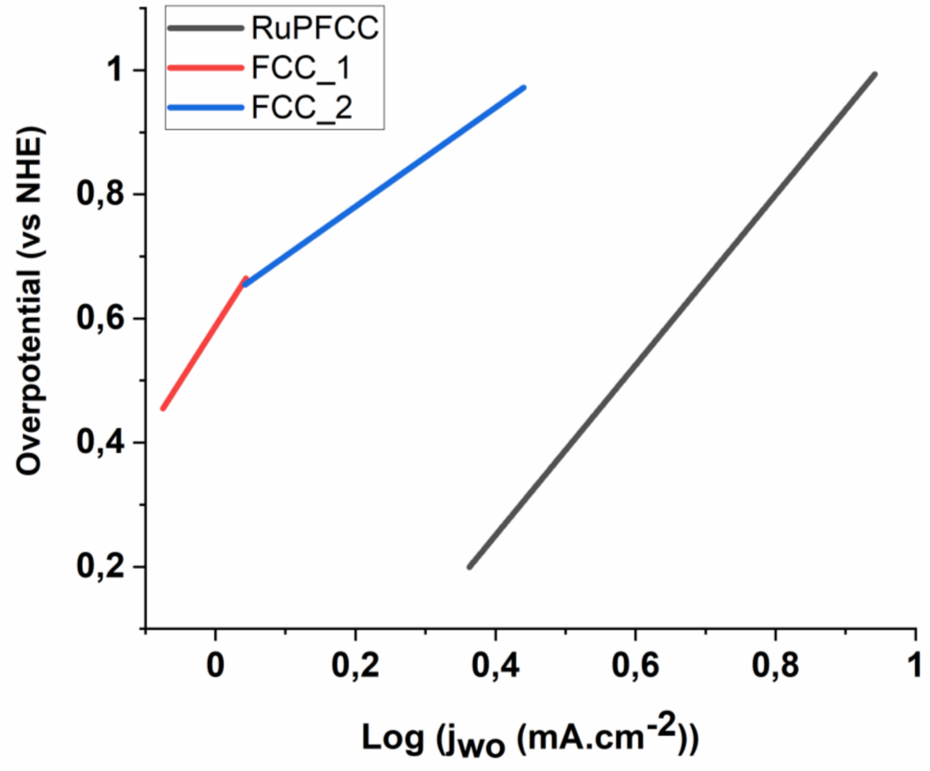

Figure S14. Tafel plots for the O_2 partial current density of two different electrodes. RuPFCC starts oxidizing water with 215 mV overpotential and shows a constant slope for the overpotential range of 0.21 V to 0.97 V. FCC_1 represents tafel slope for the overpotential range of 0.45V to 0.67V, whereas FCC_2 represents corresponding value in the overpotential range of 0.65V to 0.97 V.

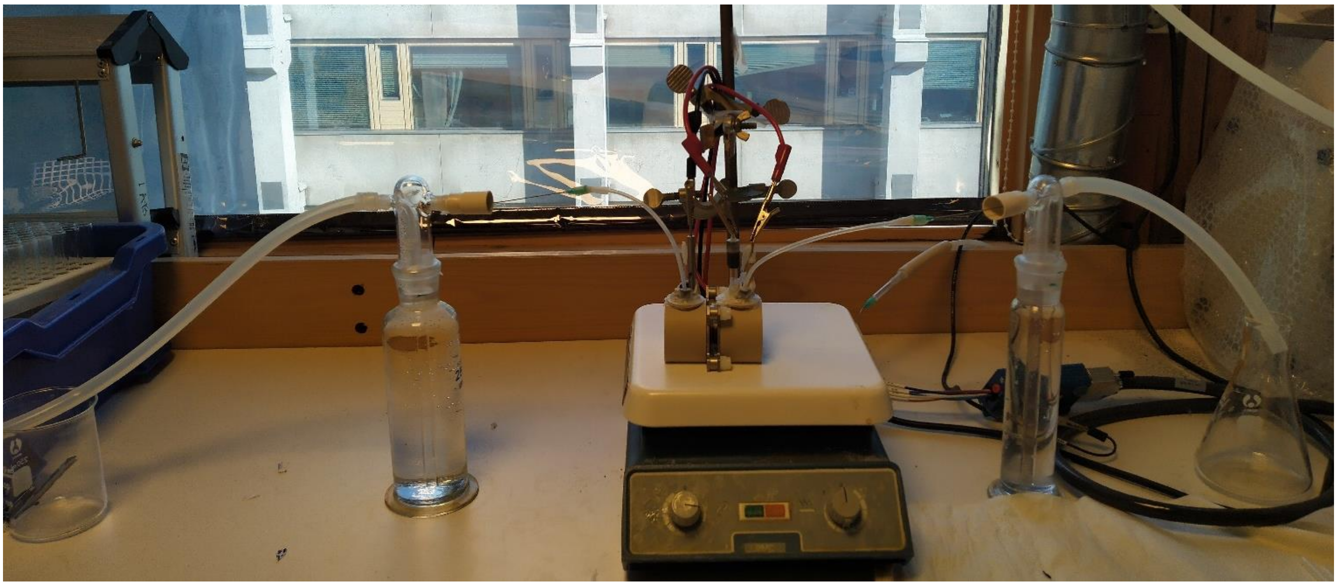

Figure S15. A graphic illustration of the home-made electrolysis set-up for the overall water electrolysis at pH 7 and quantitative gas detections from the anode (O_2) and cathode (H_2) compartments using an H-cell (purchased from redox.me). The anode and cathode compartments were separated by a Nafion-117 membrane.

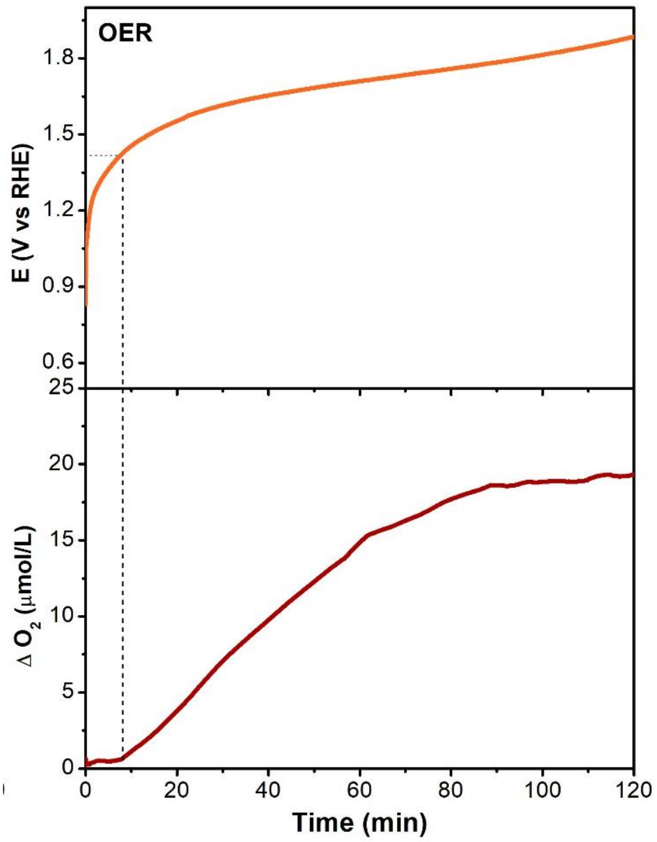

Figure S16. Dissolved oxygen detection experiment (in pH 7 phosphate buffer) at a constant current density 2.6 mA.cm^{-2} using RuPFCC (1cm x 1cm) as working electrode, a glassy carbon counter electrode and a Ag/AgCl reference electrode. Oxygen was detected using a microsensor (Unisense) immerse in the electrolyte.

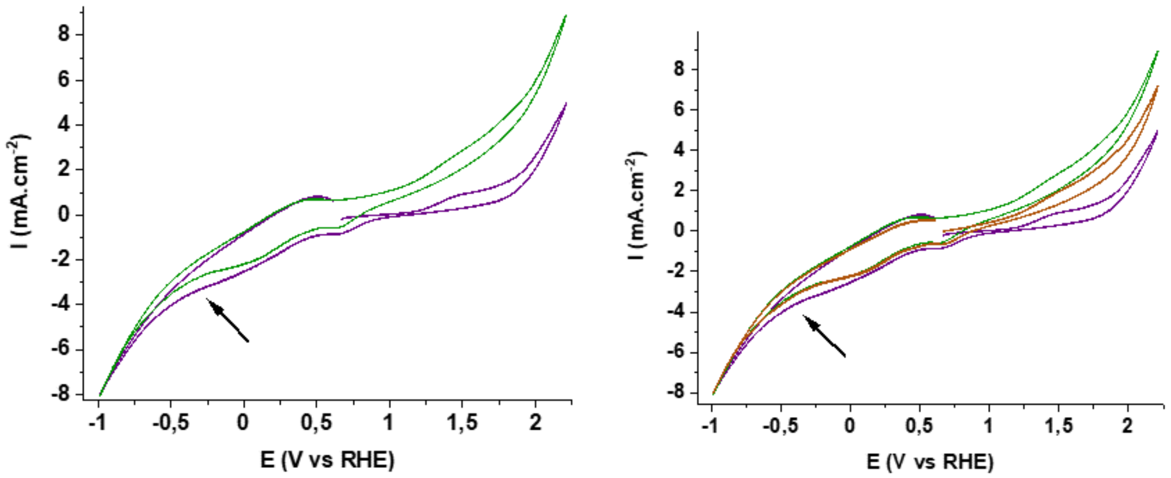

Figure S17. CVs (–1.1 V to +2.25V, vs RHE) of a pH 7 phosphate buffer (0.1 M) solution using 1cm x 0.5 cm RuPFCC (green trace) as the working electrodes (WE) at scan rate of 100 mVs^{-1}. Pt wire and Ag/AgCl (3.0 M KCl) electrodes were used as counter electrode and reference electrode respectively, before CPE experiment (green trace), after 72 h of CPE experiment at +1.71 V (purple trace) and after first regeneration experiment for 2 h (brown trace).

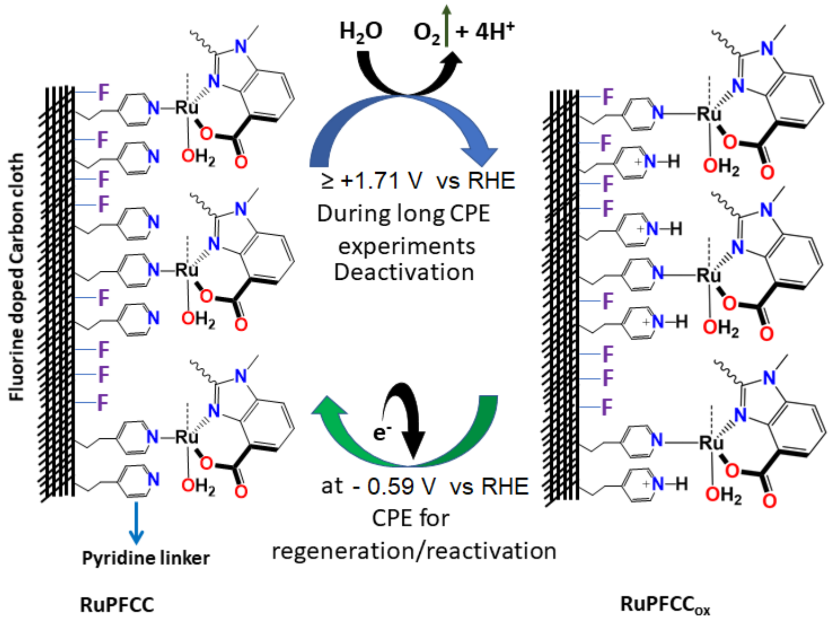

Figure S18. Possible deactivation and regeneration mechanism of RuPFCC.

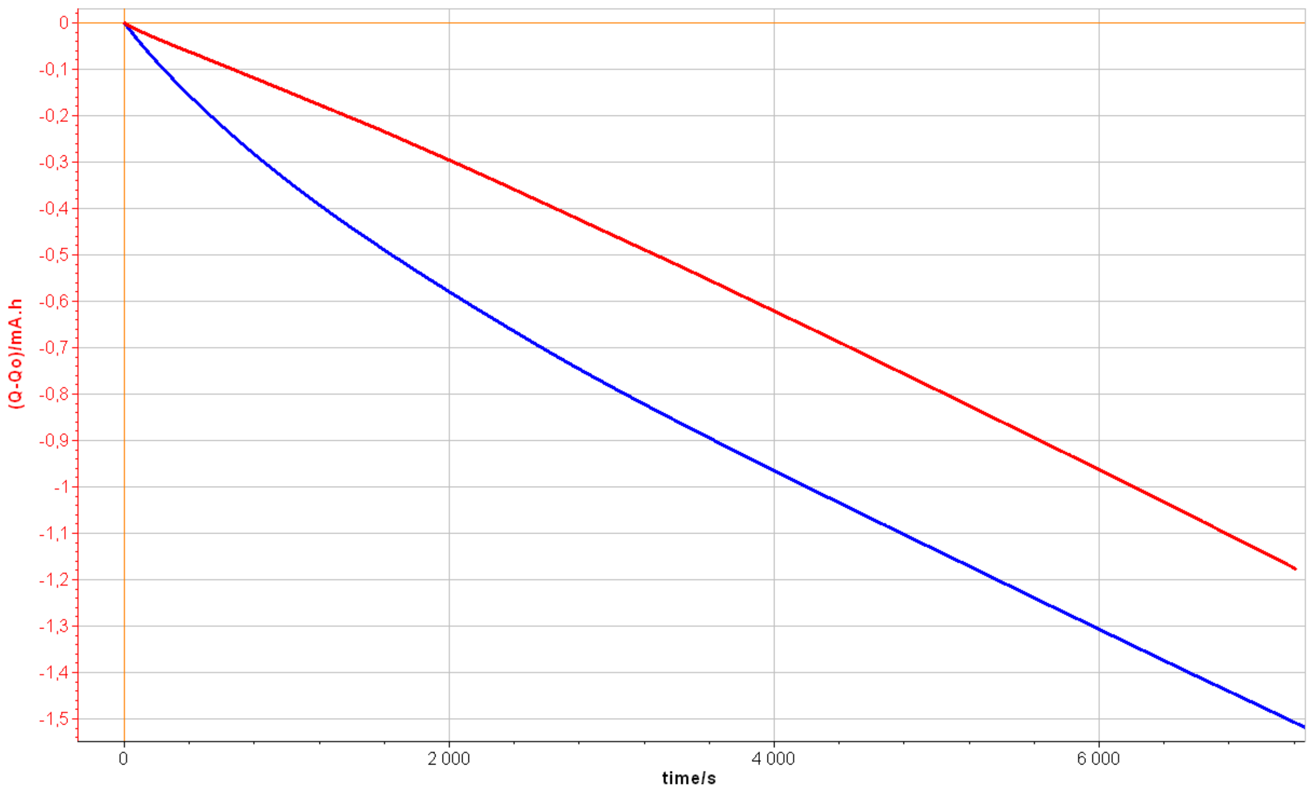

Figure S19. Negative charge (Q) vs time (s) plot for CPE over 2 h, at -1.2 V, where blue trace shows the result using 1cm × 0.5 cm RuPFCCox as working electrode, and red trace shows the result using 1cm × 0.5 cm RuPFCC as working electrode. Carbon paper (1cm x 0.5cm) and Ag/AgCl (3.0 M KCl) electrodes were used as counter electrode and reference electrode respectively.

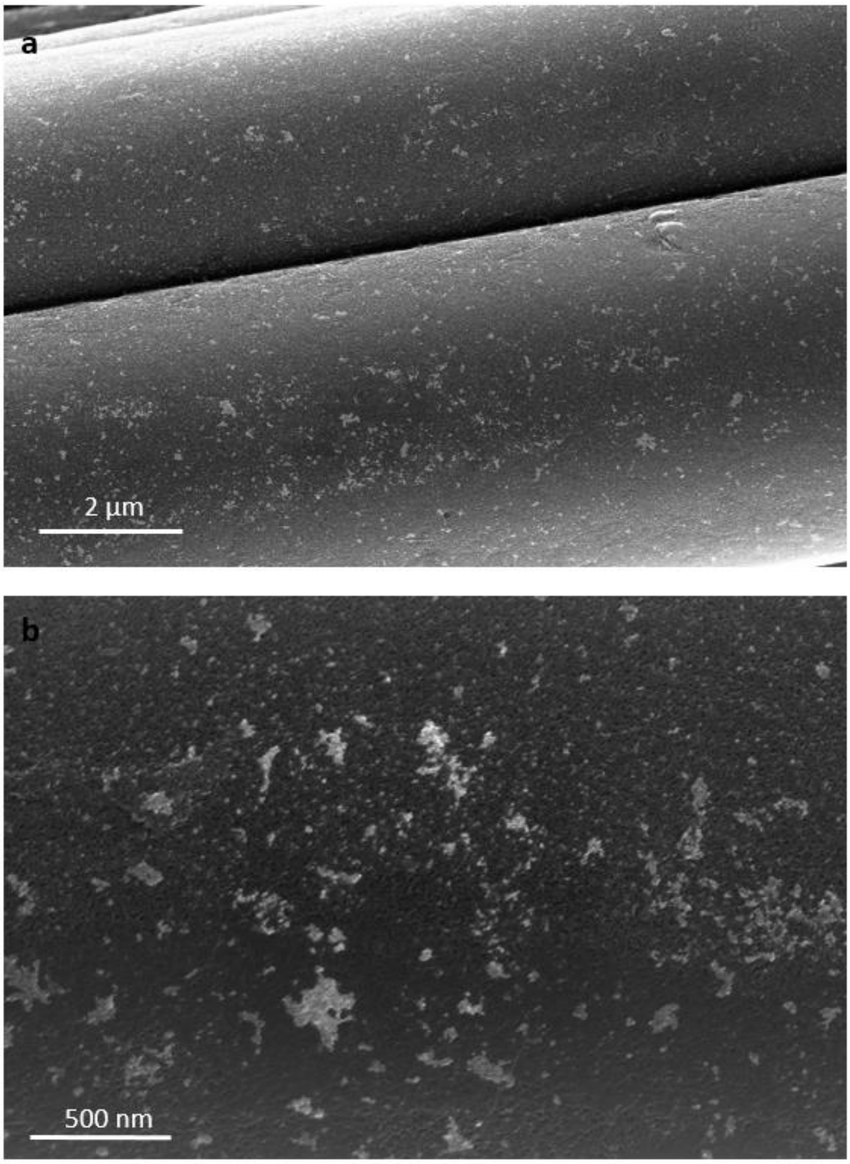

Figure S20. SEM images of the RuPFCC electrode after multiple OER and HER tests for 16 days.

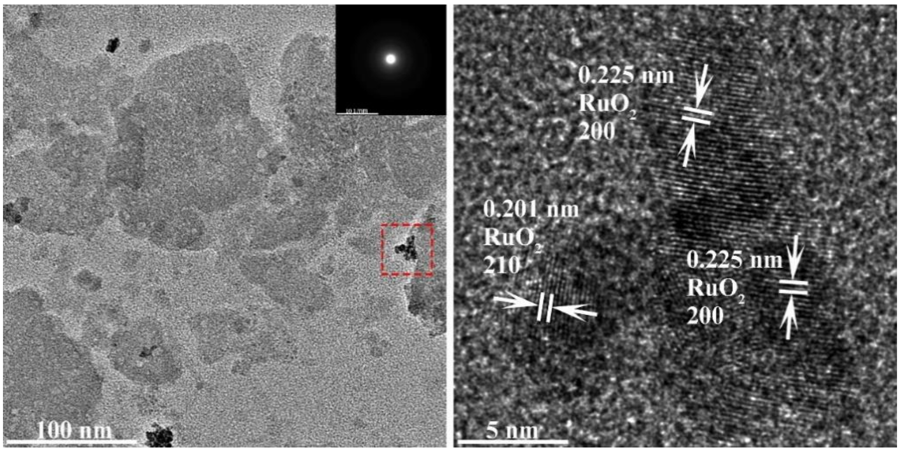

Figure S21. TEM image, SAED pattern and HRTEM of area 1 (after 16 days of multiple OER and HER experiments).

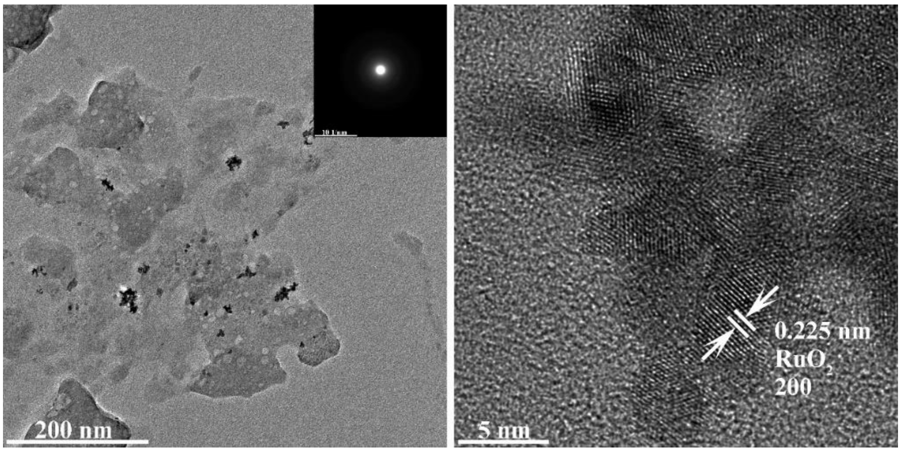

Figure S22. TEM image, SAED pattern and HRTEM of area 2 (after 16 days of multiple OER and HER experiments).

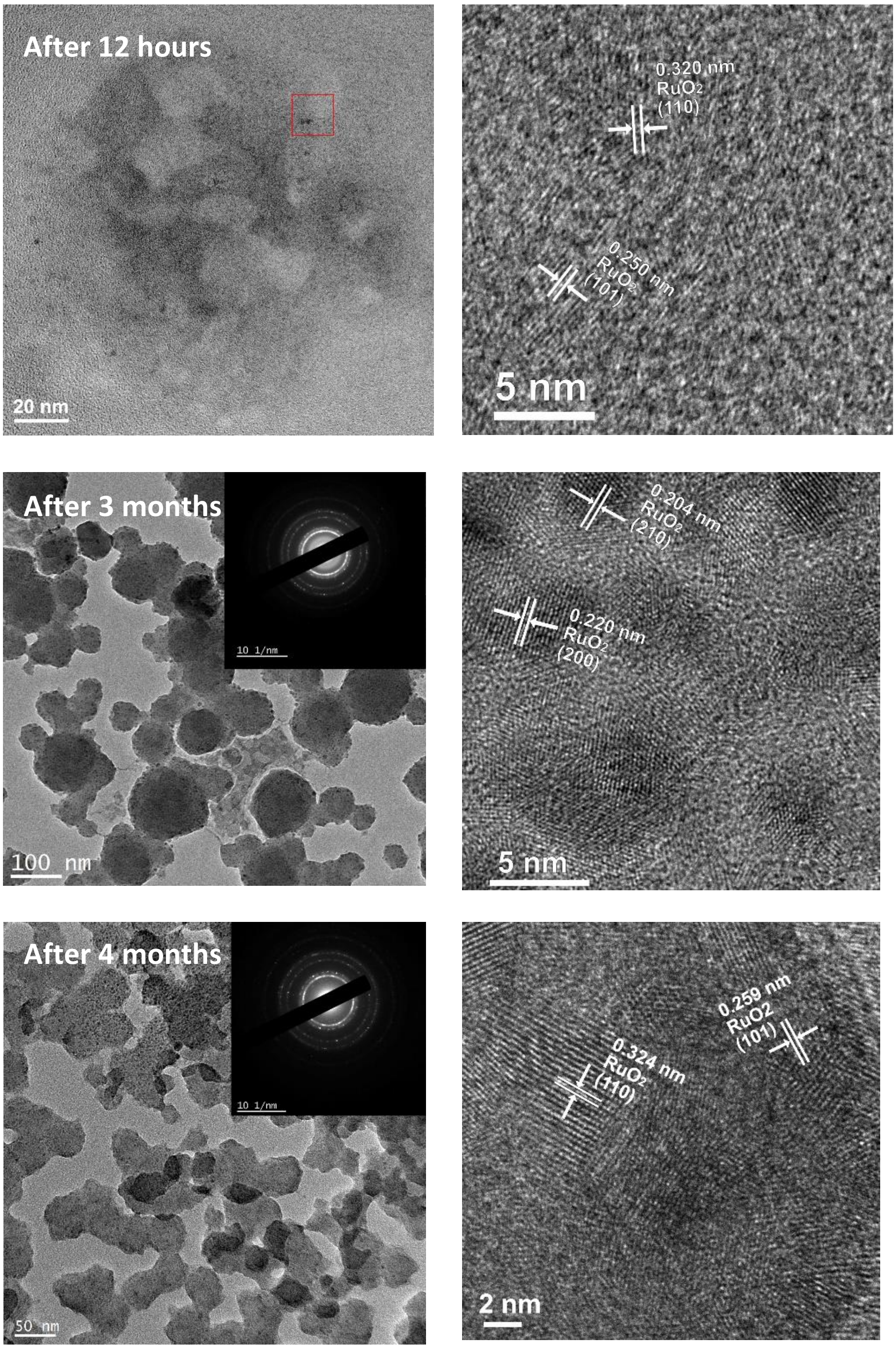

Figure S23. TEM observation of catalysts after electrolysis for 12 hours (OER), 3 months (multiple OER and HER experiments), and 4 months (multiple OER and HER experiments). Left are low-magnification and SAED patterns; Right are high-resolution images showing the oxidized product.

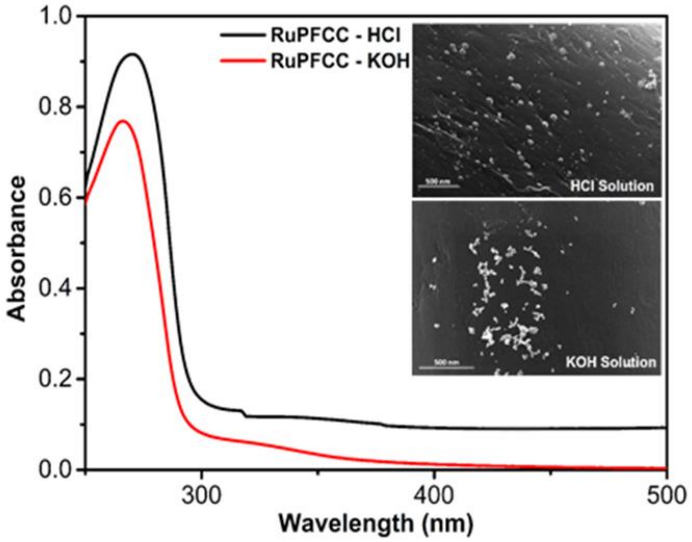

Figure S24. UV-Vis spectra of the resulting solution after immersing RuPFCC electrodes (after 16 days) in 1.0 M KOH or in 1.0 M HCl solution overnight.

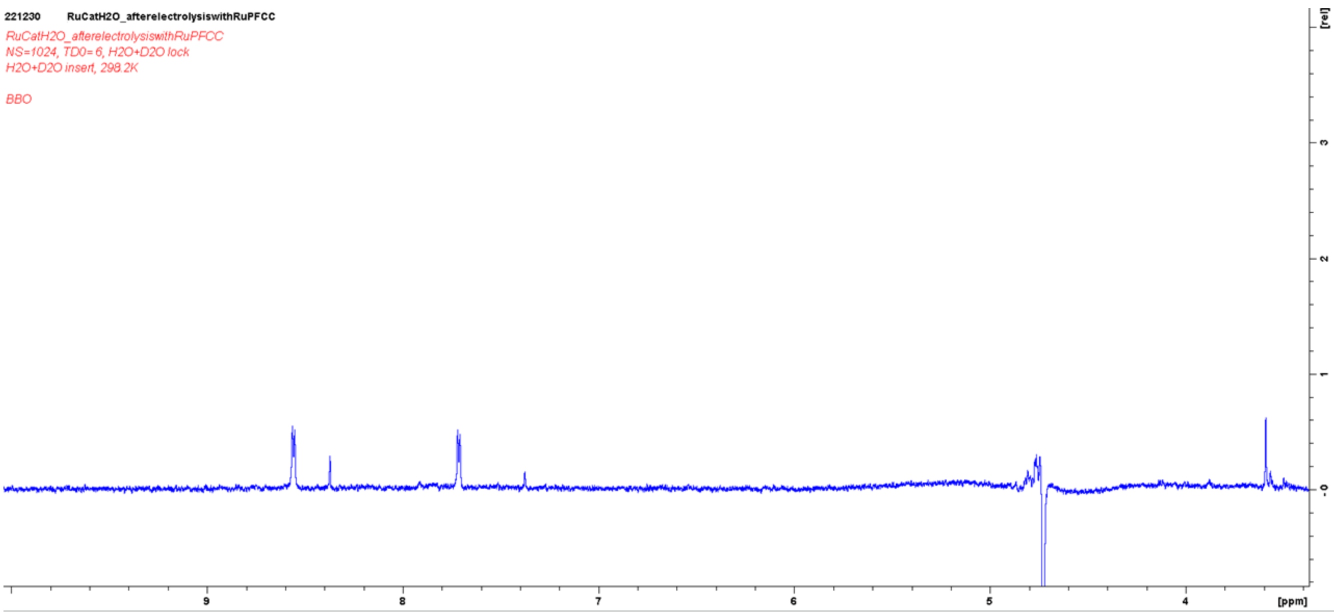

Figure S25. 500 MHz, 1H NMR (3.4-10.0 ppm) of the electrolyte solution (with 10% D_2O insert) after 4 months of multiple electrolysis experiments.

Free energy diagram for OER and HER processes:

Free Energy Diagram (eV in vacuum)

		1 H_2O	2 H_2O	1 H_2O – 1 Pyridine
	H_2O	0	0	0
	$*H_2O$	-0.69	-0.15	-0.32
HER	**H+ + e-**	0.00	0	0
	***H**	-0.20	0.12	0.65
	0.5 H_2	0.00	0	0
OER	**2 H_2O**	0.00	0.00	
	$*OH + H_2O + 0.5\ H_2$	0.22	0.96	
	$*O + H_2O + H_2$	1.64	2.52	
	$*OOH + 1.5\ H_2$	3.02	3.93	
	$O_2 + 2\ H_2$	4.92	4.92	

	H2O adsorption
1 H2O	-0.69 eV per H_2O
2 H2O	-0.42 eV per H_2O
1 H2O + 1 Pyridine	-0.32 eV per H_2O
	Pyridine adsorption
Pyridine	-1.11 eV per pyridine

Cartesian coordinates of all the optimized structures:

Ru – 1 H_2O

Ru N O C H
1 5 5 23 17

8.604159200	7.413162871	7.815788459
6.753597065	7.837702055	8.390865205
5.132335873	9.297890930	8.866169820
8.769708706	9.322946987	8.169374681
12.361359070	9.111145824	7.647240875
10.566058502	7.751522861	7.595157701
7.921305216	7.872229265	5.767607391
6.319441038	3.829939004	7.032868351
7.659335754	5.634477490	6.917854308
9.181798260	6.205210324	9.345645872
10.179854066	4.296673719	9.949173969
5.576413188	7.164545925	8.310641659
5.394575808	5.849504738	7.867197408
4.068506284	5.410248583	7.871663491
3.013724171	6.263232813	8.262567898
3.208120939	7.599759674	8.634567238
4.529727647	8.057340422	8.638591025

6.497178194	9.130568972	8.673382828
7.621218561	10.031731821	8.533489125
7.663843649	11.425891140	8.613656485
8.832170492	12.109648663	8.247781349
9.951895693	11.407543354	7.796628598
9.930792864	10.005695134	7.775896854
10.972847686	9.048523975	7.510387715
12.792597378	7.833776920	8.004670568
14.019080641	7.284424575	8.393215190
13.979830594	5.985149260	8.922031787
12.776192560	5.286808043	9.148581606
11.547357352	5.823762697	8.746361076
11.630055667	7.031128564	8.051206418
6.525298966	5.019190646	7.269475349
4.436723565	10.535392403	9.162361392
13.177537644	10.307894619	7.630103034
10.229468351	5.365448273	9.340064575
3.861001994	4.394538487	7.533969886
1.994186938	5.875448001	8.241793035
2.359046654	8.237074118	8.883297862
6.783727444	11.979302551	8.935328117
8.854935362	13.198119778	8.289326502
10.840359997	11.943963267	7.466495843
14.956515058	7.839490840	8.349701590
14.917338184	5.531501487	9.246768787
12.776605457	4.353156011	9.711115951
4.838753000	11.003317137	10.071468589
3.378148288	10.310024436	9.330059662
4.512679637	11.243876710	8.323440161
14.233153391	10.014305867	7.633757696
12.987452122	10.937043893	8.514440328
12.988251784	10.895142682	6.721121928
8.698582615	7.910869765	5.180157126
7.627864767	6.902263524	5.782761758

Ru – 1 OH

Ru	N	O	C	H
1	5	5	23	16

8.541621629	7.472269869	7.697344496
6.745017038	7.891377366	8.394098476
5.109985859	9.326506264	8.880587245
8.714672534	9.391711333	8.116316103
12.311333195	9.129673273	7.655579175
10.514105992	7.801442899	7.656806106
8.267073180	8.103436589	5.858351318
6.359739007	3.905704307	6.971412021
7.662693156	5.731082334	6.905714351
9.136176402	6.158647688	9.228537945
10.135763586	4.249696226	9.864826026
5.578861171	7.192668004	8.338359987

5.413154542	5.885198120	7.877403544
4.093324533	5.427326646	7.881369185
3.030003225	6.261208834	8.288106104
3.208367567	7.598306695	8.667712027
4.524175423	8.071080356	8.671590123
6.468314599	9.187231906	8.662057559
7.578873094	10.094509813	8.496572077
7.631216288	11.488818742	8.604342129
8.809088762	12.163773456	8.263913080
9.933948391	11.455773911	7.831174754
9.886222195	10.057377171	7.774899890
10.930077562	9.086238071	7.554159376
12.740075828	7.836032827	7.979698790
13.973399331	7.260278590	8.297555044
13.936480323	5.943184677	8.780645905
12.733609285	5.247133994	9.025791118
11.496719971	5.807101778	8.690853861
11.571125066	7.048578692	8.060490722
6.552692595	5.090556832	7.248419560
4.396103838	10.562123567	9.144861613
13.147584315	10.312820638	7.601347237
10.170166012	5.325242749	9.261767011
3.900090018	4.414974605	7.525532935
2.015650888	5.860272727	8.267112379
2.351636230	8.225537173	8.915582230
6.757165489	12.046232379	8.935714228
8.846390614	13.250398295	8.329955703
10.842117423	11.986170231	7.549486191
14.917130428	7.801045028	8.223221161
14.880615172	5.465886135	9.046417678
12.745598979	4.286520502	9.541747147
4.770960792	11.046536744	10.056714053
3.335696983	10.330410575	9.287264711
4.489032134	11.256582441	8.296697890
14.196473498	9.999648021	7.565513391
13.001630432	10.945979325	8.490330929
12.932223221	10.897788620	6.697440452
7.906534999	7.305450965	5.416874862

Ru – 1 H

Ru	N	O	C	H
1	5	4	23	16

8.543607063	7.380523751	8.171409767
6.632961873	7.952718711	8.345232240
4.983988233	9.434787864	8.665695887
8.641224550	9.391952407	8.289361128
12.281007474	9.166274114	7.860691667
10.514419585	7.812832847	8.100162159
6.211011136	3.889769225	7.196542180
7.617759895	5.606609552	7.456808442

9.375328074	5.769096303	9.293558125
10.575599560	3.923054476	9.726239612
5.449678945	7.268842937	8.283865416
5.265373982	5.918729673	7.989444989
3.942579869	5.472758388	8.011424571
2.879785789	6.356075852	8.291385761
3.072102719	7.722341101	8.531369107
4.393460839	8.179299890	8.515221043
6.350754576	9.259147859	8.539501611
7.479489034	10.137958081	8.472927841
7.527253122	11.535281420	8.498948195
8.739344439	12.193390980	8.272224593
9.897376949	11.452133622	8.022924930
9.844237359	10.055376057	8.048544147
10.901134262	9.094850764	7.942668065
12.767918939	7.868481832	8.032749528
14.048371505	7.310315572	8.087476027
14.122902037	5.943163118	8.386465107
12.986558383	5.163147662	8.684781270
11.703296549	5.711864982	8.635417859
11.635585352	7.045902700	8.231714296
6.425851534	5.058254170	7.540667703
4.280575307	10.688192406	8.854846511
13.089350150	10.365270977	7.753329939
10.480024345	5.047911164	9.226141574
3.751279828	4.424263809	7.780434802
1.861141805	5.965841750	8.299182459
2.222626317	8.382026464	8.709909845
6.618903774	12.105753580	8.679090869
8.779297456	13.281706606	8.280502134
10.840967583	11.955828830	7.823657675
14.954113461	7.896183174	7.930178582
15.107610554	5.476309825	8.436432184
13.092637647	4.127851742	9.010275466
4.645312690	11.211372827	9.749214198
3.215629524	10.473910594	8.992481040
4.392154203	11.343076535	7.977888445
14.137984539	10.069313293	7.644727561
12.995721823	10.989110081	8.655070321
12.804431583	10.953688479	6.870818016
8.515987385	7.633000500	6.625666270

Ru – 1 OOH

Ru	N	O	C	H
1	5	6	23	16

8.565644790	7.515185030	7.605022152
6.740135445	7.915881369	8.227421343
5.126314239	9.337788415	8.795990387
8.749097172	9.417520012	8.063102035

12.353865511	9.151654815	7.684091284
10.557492195	7.821507605	7.544458908
8.321929036	8.243600766	5.801246741
8.019424452	7.308550960	4.772207976
6.314954703	3.930679352	6.796081689
7.666665983	5.724378637	6.772751046
9.138525080	6.230473483	9.128127522
10.062269217	4.269078868	9.721156144
5.578143828	7.216329227	8.196388732
5.410381533	5.898909308	7.761482696
4.097125538	5.427991397	7.837080750
3.045067108	6.256416745	8.285132853
3.224918075	7.598411879	8.645942814
4.534244362	8.084884968	8.583055718
6.479589564	9.201422629	8.546843601
7.603112503	10.109913094	8.433860724
7.657007981	11.500156425	8.577487487
8.847546334	12.176748354	8.283244110
9.978552379	11.479493279	7.850922601
9.930604708	10.081702818	7.754900516
10.975485785	9.110414108	7.515397358
12.767580521	7.850821990	7.989203915
13.982213899	7.266210065	8.363408204
13.919231418	5.939736464	8.816253049
12.703226072	5.244451796	8.990131055
11.487297817	5.816041130	8.603484322
11.595884516	7.062320585	7.983306412
6.530812971	5.101814483	7.102848522
4.417692409	10.564904089	9.109737270
13.192830515	10.334404962	7.702967605
10.143790252	5.353980253	9.144841360
3.895433819	4.406831648	7.512214392
2.036683812	5.842345678	8.324265302
2.375677521	8.214884821	8.941366083
6.775460356	12.054136222	8.894012279
8.885579249	13.261702005	8.375621986
10.889564652	12.017494222	7.594463224
14.927984656	7.808748956	8.360489832
14.846795506	5.455547702	9.125218950
12.685466272	4.280506382	9.499717886
4.811458349	11.025200681	10.026052526
3.360701427	10.327797302	9.267985293
4.491386366	11.281241281	8.278316132
14.241560288	10.021255211	7.655824169
13.042809074	10.918384474	8.624527699
12.985025699	10.967866789	6.830830374
7.815469639	6.473826644	5.310784165

Ru – 1 O

Ru	N	O	C	H
1	5	5	23	15

8.532994563	7.548052158	7.485667463
6.783914293	7.909770231	8.353493448
5.136175750	9.313912251	8.846881256
8.691571205	9.455495435	7.962177451
12.306514320	9.146296299	7.653183457
10.482099937	7.866334375	7.676306999
8.417041702	7.913296842	5.762212943
6.375742034	3.851779756	7.016387094
7.706468083	5.656372794	6.876015815
9.052945632	6.238374059	9.121600874
9.994077831	4.342052216	9.880145030
5.634213549	7.174873578	8.329448075
5.474108796	5.861373568	7.881537088
4.156633999	5.397542199	7.915541643
3.088723785	6.218658224	8.336404606
3.259263662	7.558537260	8.704765618
4.570448313	8.039788377	8.675682508
6.481047770	9.204423320	8.601151323
7.570797428	10.135346116	8.415667774
7.626609742	11.513476274	8.600726013
8.816556189	12.203983880	8.307198019
9.949812261	11.510071180	7.881559301
9.893993414	10.118704796	7.732683780
10.927888946	9.141889669	7.549307835
12.701294864	7.843470854	7.992750779
13.919301977	7.244352001	8.324297314
13.853797688	5.928709107	8.809853798
12.637029266	5.252902793	9.039066542
11.413978537	5.835528956	8.692351267
11.515983709	7.079975201	8.073787053
6.606171910	5.045167228	7.244306922
4.409403435	10.531901724	9.157281844
13.167176019	10.310876363	7.584378605
10.064115494	5.390264235	9.232818485
3.970809745	4.380727996	7.567732060
2.078448806	5.806843718	8.333981449
2.403961949	8.182604373	8.964026422
6.756158072	12.054243366	8.967558260
8.857730257	13.285211004	8.431973941
10.877584757	12.044336450	7.681438159
14.873373794	7.767272401	8.256517519
14.786760797	5.436344069	9.087339565
12.625473375	4.290293088	9.551465254
4.792536623	10.991058276	10.078795552
3.354528551	10.281690029	9.306481410
4.485094586	11.251239606	8.329328517
14.208384794	9.976619864	7.526801026
13.051500818	10.946162907	8.476526971
12.943934602	10.899897531	6.684792213

Ru – 2 H_2O

Ru	N	O	C	H
1	5	6	23	19

8.728200814	7.582740381	8.409840672
6.659585410	7.912752602	8.317768016
5.027957915	9.455281384	8.515341148
8.685960640	9.501668222	8.269603477
12.385552825	9.301822167	8.033585345
10.629861887	7.964967112	8.349605272
8.583228962	7.162178409	6.460056219
5.717242239	3.622527094	7.726929548
7.101880290	5.040925793	6.723534319
9.334651172	5.580276903	9.071780667
10.697020588	3.821228520	9.389763186
8.692446866	7.508930816	10.613517617
5.442392338	7.260157137	8.197678105
5.126167267	5.906638989	7.937435932
3.768893145	5.570289501	8.015788730
2.761755660	6.513374198	8.271988119
3.057600536	7.864994432	8.436117465
4.407466262	8.218527062	8.383722637
6.386716395	9.242117921	8.434892478
7.485614245	10.186199595	8.397596026
7.488522855	11.587655578	8.424403974
8.696835913	12.281250550	8.283923088
9.903566615	11.586691268	8.143774746
9.904233661	10.188866474	8.148565589
11.001962710	9.245722324	8.145255837
12.866148973	7.996777582	8.186531048
14.135477503	7.406780598	8.150997271
14.186144283	6.020828054	8.350058680
13.042042770	5.233620863	8.604243863
11.765609967	5.798925042	8.646095308
11.734173200	7.177968658	8.403958120
6.042328377	4.780058387	7.485158876
4.337085354	10.716244722	8.708276968
13.192177208	10.484394813	7.805399945
10.527822735	4.992240227	9.043446548
3.512448105	4.524486845	7.849525620
1.724185083	6.182736090	8.319172015
2.266054930	8.597214069	8.596501290
6.560366016	12.143585502	8.537194920
8.697114884	13.369000036	8.290611845
10.843122042	12.131982423	8.049556566
15.050143803	7.975799920	7.981406115
15.158449663	5.529603591	8.321787934
13.134711913	4.162895106	8.789529229
4.701879047	11.231937571	9.606470945
3.267535913	10.513999652	8.838799197
4.458985633	11.373172395	7.835182489
14.225303369	10.172123021	7.610471480

13.189846139	11.147022108	8.683270894
12.830494330	11.038026335	6.929351124
9.409214677	6.747514016	6.145998886
7.933873342	6.421456381	6.646516266
7.770711573	7.512894548	10.930439787
8.948673040	6.544366702	10.505577620

References:

1. G. Kresse, J. Furthmuller, Efficiency of ab-initio total energy calculations for metals and semiconductors using a plane-wave basis set, *Comput. Mater. Sci*. **1996**, 6, 15-50.
2. G. Kresse, J. Furthmuller, Efficient iterative schemes for ab initio total-energy calculations using a plane-wave basis set, *Phys. Rev. B*. **1996**, 54, 11169-11186.
3. P.E. Blochl, Projector augmented-wave method, Phys. Rev. B *Condens. Matter*. **1994**, 50 17953-17979.
4. G. Kresse, D. Joubert, From ultrasoft pseudopotentials to the projector augmented wave method, *Phys. Rev. B*, **1999**, 59, 1758-1775.
5. J.P. Perdew, K. Burke, M. Ernzerhof, Generalized Gradient Approximation Made Simple, *Phys. Rev. Lett.* **1996**, 77, 3865-3868.
6. S. Grimme, J. Antony, S. Ehrlich, H. Krieg, A consistent and accurate ab initio parametrization of density functional dispersion correction (DFT-D) for the 94 elements H-Pu, J. *Chem. Phys.* **2010**, 132 154104.
7. H. Peng, M.T. Tang, X. Liu, P.S. Lamoureux, M. Bajdich, F. Abild-Pedersen, The role of atomic carbon in directing electrochemical CO2 reduction to multicarbon products, *Energy Environ. Sci.* **2021**, 14, 473-482.
8. Lee, L. Z.; Ahmad Zaini, M. A., Metal chloride salts in the preparation of activated carbon and their hazardous outlook. *Desalination and Water Treatment* **2016,** *57*, 16078-16085.
9. Ganiyu, S. A.; Alhooshani, K.; Sulaiman, K. O.; Qamaruddin, M.; Bakare, I. A.; Tanimu, A.; Saleh, T. A., Influence of aluminium impregnation on activated carbon for enhanced desulfurization of DBT at ambient temperature: Role of surface acidity and textural properties. *Chemical Engineering Journal* **2016,** *303*, 489-500.
10. Alvarado Ávila, M. I.; Toledo-Carrillo, E.; Dutta, J., Improved chlorate production with platinum nanoparticles deposited on fluorinated activated carbon cloth electrodes. *Cleaner Engineering and Technology* **2020,** *1*, 100016.
11. Park, M.-S.; Lee, Y.-S., Functionalization of graphene oxide by fluorination and its characteristics. *Journal of Fluorine Chemistry* **2016,** *182*, 91-97.
12. Bokobza, L.; Bruneel, J.-L.; Couzi, M., Raman Spectra of Carbon-Based Materials (from Graphite to Carbon Black) and of Some Silicone Composites. *C* **2015,** *1* (1).
13. Bahuguna, G.; Chaudhary, S.; Sharma, R. K.; Gupta, R., Electrophilic Fluorination of Graphitic Carbon for Enhancement in Electric Double-Layer Capacitance. *Energy Technology* **2019,** *7*, 1900667.
14. Henry, D. G.; Jarvis, I.; Gillmore, G.; Stephenson, M., Raman spectroscopy as a tool to determine the thermal maturity of organic matter: Application to sedimentary, metamorphic and structural geology. *Earth-Science Reviews* **2019,** *198*, 102936.
15. Kordek, K.; Jiang, L.; Fan, K.; Zhu, Z.; Xu, L.; Al-Mamun, M.; Dou, Y.; Chen, S.; Liu, P.; Yin, H.; Rutkowski, P.; Zhao, H., Two-Step Activated Carbon Cloth with Oxygen-Rich Functional Groups as a High-Performance Additive-Free Air Electrode for Flexible Zinc–Air Batteries. *Advanced Energy Materials* **2019,** *9* (4), 1802936.

16. Li, L.; Yao, X.; Li, H.; Liu, Z.; Ma, W.; Liang, X., Thermal stability of oxygen-containing functional groups on activated carbon surfaces in a thermal oxidative environment. *Journal of Chemical Engineering of Japan* **2014,** *47*, 21-27.
17. Avilés, F.; Cauich-Rodríguez, J. V.; Moo-Tah, L.; May-Pat, A.; Vargas-Coronado, R., Evaluation of mild acid oxidation treatments for MWCNT functionalization. *Carbon* **2009,** *47*, 2970-2975.
18. Berenguer, R.; Ruiz-Rosas, R.; Gallardo, A.; Cazorla-Amorós, D.; Morallón, E.; Nishihara, H.; Kyotani, T.; Rodríguez-Mirasol, J.; Cordero, T., Enhanced electro-oxidation resistance of carbon electrodes induced by phosphorus surface groups. *Carbon* **2015,** *95*, 681-689.
19. Zhao, Z.; Yang, Z.; Hu, Y.; Li, J.; Fan, X., Multiple functionalization of multi-walled carbon nanotubes with carboxyl and amino groups. *Applied Surface Science* **2013**, 276, 476-481.
20. A. Shatskiy, A. A. Bardin, M. Oschmann, R. Matheu, J. Benet-Buchholz, L. Eriksson, M. D. Kärkäs, E. V. Johnston, C. Gimbert-Suriñach, A. Llobet, B. Åkermark, *ChemSusChem* **2019**, 12, 2251–2262.